**Proceedings of ASME Turbo Expo 2024**
**Turbomachinery Technical Conference and Exposition**
**GT2024**
**June 24-28, 2024, London, United Kingdom**

**GT2024-125914**

# REVERSIONARY CONTROL MODES FOR THE MITIGATION OF FAILURES IN A PARTIALLY TURBOELECTRIC AIRCRAFT PROPULSION SYSTEM

**Donald L. Simon**
NASA Glenn Research Center
Cleveland, OH, USA

**Amy K. Chicatelli**
HX5, LLC
Brook Park, OH, USA

**Santino J. Bianco**
NASA Glenn Research Center
Cleveland, OH, USA

**Marcus A. Horning**
HX5, LLC
Brook Park, OH, USA

**Joseph R. Saus**
NASA Glenn Research Center
Cleveland, OH, USA

## ABSTRACT

*In support of emission and fuel burn reduction goals, the aviation industry is actively pursuing the advancement of electrified aircraft propulsion (EAP) technology. This includes turboelectric and hybrid electric propulsion designs that combine gas turbine engine and electrical system hardware. Such architectures exhibit a high degree of coupling between subsystems. This drives the need for system-level control strategies to ensure the safe, coordinated, and efficient operation of all subsystems. The design and certification of any aircraft propulsion system requires that all potential subsystem failures are identified, and the hazards posed by these failures are appropriately mitigated. This requirement is particularly challenging for EAP systems due to their integrated nature. One approach to assist in EAP failure mitigation is the inclusion of automated reconfiguration capabilities within the propulsion control system. Such control modes, referred to as reversionary control modes, are designed to automatically detect failures and activate backup control modes upon failure detection. This paper covers the design and evaluation of reversionary control mode logic developed for a partially turboelectric propulsion concept. Test results from a real-time hardware-in-the-loop evaluation of the concept are also presented and discussed. The results show that the developed reversionary control logic can successfully detect and mitigate subsystem failures in a representative environment that includes actual electrical system hardware.*

Keywords: Electrified Aircraft Propulsion, Aircraft Propulsion Controls, Reversionary Control Modes

## NOMENCLATURE

***Acronyms***

| | |
|---|---|
| ASMICS | Adaptive sliding mode impedance controller with scaling |
| DC | Direct current |
| EAP | Electrified aircraft propulsion |
| HIL | Hardware-in-the-loop |
| HP | High-pressure |
| HPC | High-pressure compressor |
| HPX | Horsepower extraction |
| HyPER | Hybrid Propulsion Emulation Rig |
| LP | Low-pressure |
| LPC | Low-pressure compressor |
| NPSS | Numerical propulsion system simulation |
| PI | Proportional plus integral |
| PLA | Power lever angle |
| SLS | Sea level static |
| STARC-ABL | Single-aisle turboelectric aircraft with aft boundary layer propulsion |
| T-MATS | Toolbox for the modeling and analysis of thermodynamic systems |
| VAFN | Variable area fan nozzle |
| VBV | Variable bleed valve |

***Parameters***

| | |
|---|---|
| $A$, $B$, $C$ | State-space matrices |
| $N_{1c}$ | Corrected turbofan fan speed |
| $\dot{N}_{1c}$ | Corrected turbofan fan speed derivative |
| $N_{2c}$ | Corrected turbofan low-pressure shaft speed |
| $\dot{N}_{2c}$ | Corrected turbofan low-pressure shaft speed derivative |
| $N_{3c}$ | Corrected turbofan core speed |
| $\dot{N}_{3c}$ | Corrected turbofan core speed derivative |

| | |
|---|---|
| $N_{tc}$ | Corrected tailfan speed |
| $\dot{N}_{tc}$ | Corrected tailfan speed derivative |
| $Ps3$ | Turbofan HPC exit static pressure |
| $Q_m$ | Tailfan motor torque |
| $T4$ | Turbine inlet temperature |
| $u,x,y$ | State-space input, state, and output vectors |
| $W_f$ | Fuel flow |
| $\gamma$ | Ratio of tailfan to turbofan speed variation |
| $\Delta$ | Deviation about trim condition |

## 1. INTRODUCTION

Electrified aircraft propulsion (EAP) relies on the use of electrical power to produce aircraft thrust. It holds great potential for the reduction of aircraft fuel burn, emissions, and noise. Currently, NASA and other organizations are actively working to advance technologies necessary to bring EAP designs to reality [1,2]. This includes turboelectric and hybrid electric designs that combine gas turbine engines and electrical components. A requirement for the development of any civil aircraft is that all potential hazards in the design are identified and appropriately mitigated to ensure that the system is safe [3,4]. EAP designs will introduce new flight critical propulsion components and architectures, often with a high degree of coupling between subsystems. This raises the concern of cascading failure scenarios where one subsystem failure causes subsequent failures throughout the architecture. Such scenarios must be identified and shown to be appropriately mitigated as part of the aircraft safety assessment and design process [5,6].

To facilitate failure mitigation, redundancy within an EAP architecture will be required to assure that the propulsion system can continue to deliver adequate thrust in the event of a failure. Passive hardware fault management techniques such as circuit breakers, current limiters, and power electronics technology will also be critical [7,8]. Additionally, the propulsion control system is expected to play a significant role in assuring that EAP systems comply with the airworthiness standards set forth by regulatory agencies. This includes logic to automatically detect system failures and revert to alternate backup control modes to enable safe failure mitigation. Such backup control modes are common in modern aircraft engine electronic control systems and are often referred to as "reversionary" control modes (e.g., see Refs. [9,10,11]). Compared to conventional aircraft engines, EAP systems are expected to present unique reversionary control development needs due to their complex integrated nature.

Past NASA efforts focused on the development of EAP system reversionary control strategies have considered both parallel hybrid and partially turboelectric designs. Reference [12] focused on a parallel hybrid architecture consisting of a two-spool turbofan engine with electric machines attached to the high-pressure (HP) and low-pressure (LP) shafts, a high voltage direct current (DC) power bus, and an energy storage device. This study demonstrated that reversionary control strategies could prevent engine overtemperature events and reduce the risk of compressor stalls. References [6,13] presented reversionary control strategies for the NASA Single-aisle Turboelectric AiRCraft with Aft Boundary Layer propulsor (STARC-ABL) concept aircraft. The STARC-ABL is a partially turboelectric design consisting of two wing mounted geared turbofan engines and an electric motor driven boundary layer ingesting tailfan propulsor [14,15]. It exhibits coupling between subsystems and past analysis has shown that unmitigated subsystem failures in this concept can cascade into catastrophic events [6]. The STARC-ABL reversionary control study in Ref. [6] was preliminary in nature and only considered failure mitigation at a single flight condition. Reference [13] considered a modified STARC-ABL concept that included energy storage and applied the NASA-developed Turbine Electrified Energy Management control concept [16]. Neither Ref. [6] nor Ref. [13] considered failure detection and mitigation during transient operation. Follow-on NASA work has added several enhancements to the STARC-ABL reversionary control logic. This includes the addition of failure detection logic and an integrated control design approach that in combination provide robust full-flight envelope detection and mitigation of potential STARC-ABL subsystem failures. Initial results from a flight simulator evaluation of the STARC-ABL reversionary control logic were presented in Ref. [17]. This paper provides details regarding the logic's overall design and operation.

The remaining sections of this paper are organized as follows. An overview of the STARC-ABL concept is provided in Section 2 and a description of its baseline propulsion control design is given in Section 3. This is followed by a description of STARC-ABL failure modes and effects in Section 4. Section 5 discusses reversionary control logic including failure detection logic and the reversionary control modes. Section 6 presents results from a real-time hardware-in-the-loop (HIL) test conducted to evaluate the effectiveness of the reversionary control fault mitigation strategy at select operating points. This test included a subscale representation of the STARC-ABL's electrical system and simulated turbomachinery elements. Finally, a discussion is provided in Section 7 followed by conclusions in Section 8.

## 2. STARC-ABL OVERVIEW

An image of the STARC-ABL aircraft and a block diagram of its propulsion system are provided in Fig. 1 and Fig. 2, respectively. The two turbofan engines in this single-aisle commercial airliner concept serve the dual purpose of producing thrust and supplying mechanical offtake power delivered to electric generators attached to their LP shafts. Electrical power produced by the generators is transported over a 1000V DC bus to a motor controller and inverter. The motor controller operates a 3500 hp motor that drives the tailfan. The end-to-end efficiency of the STARC-ABL's electrical system is approximately 90%. System inputs include fuel flow supplied to each turbofan and torque commands provided to each generator controller and the tailfan motor controller. Additionally, each turbofan is equipped with a variable bleed valve (VBV) installed between its low-pressure compressor (LPC) and high-pressure compressor (HPC) and a variable area fan nozzle (VAFN) installed in its bypass stream. The tailfan is also equipped with a VAFN actuator, which is installed aft of its fan module.

**Figure 1:** STARC-ABL AIRCRAFT.

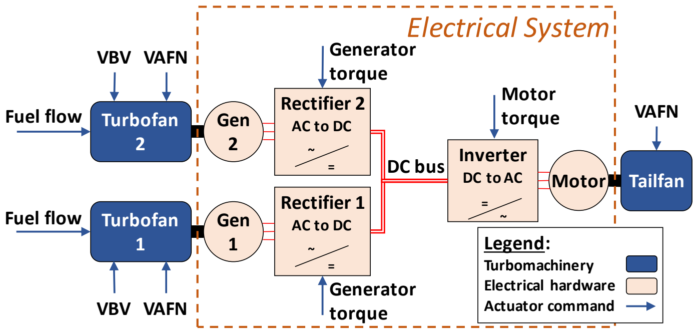


**Figure 2:** STARC-ABL PROPULSION SYSTEM.

## 3. BASELINE STARC-ABL CONTROL DESIGN

Original NASA publications on the STARC-ABL concept (Refs. [14,15]) are system studies focused on steady-state performance benefits. They are based on a nonlinear steady-state model of the STARC-ABL coded in the Numerical Propulsion System Simulation (NPSS) environment [18] and do not explicitly discuss transient operation or a control concept of operations for the propulsion system. To address this need, a system-level integrated control design for the STARC-ABL propulsion system has been developed as detailed in Ref. [19]. This design has been shown to promote coordinated operation of the tailfan and turbofan subsystems during both steady-state and transient operation under nominal (failure free) conditions. It will serve as the "baseline" architecture that the reversionary control developed in this study will be compared against. An overview of the transient propulsion system model used for developing and evaluating the baseline control is given in Section 3.1, followed by a discussion of the design's variable geometry and thrust schedules in Section 3.2, and its closed-loop control strategy in Section 3.3.

### 3.1 Nonlinear Transient Propulsion System Model

The baseline control presented in Ref. [19] was designed and evaluated using a nonlinear transient model of the STARC-ABL propulsion system derived from the steady-state NPSS model used in Ref. [15]. The transient model is implemented in MATLAB® Simulink® (MathWorks, Natick, MA) using the NASA-developed Toolbox for the Modeling and Analysis of Thermodynamic Systems (T-MATS) [20] and a power flow modeling approach [21]. T-MATS is used to model the turbomachinery components, while the power flow approach is used to model electrical system components at turbomachinery time-scales. Shaft dynamics are also included to enable simulation of transient operation.

### 3.2 Variable Geometry and Thrust Schedules

The baseline controller applies schedules for the VBV and VAFN variable geometry actuators consistent with those of the original NPSS model. The turbofan VBV is open-loop scheduled based on turbofan corrected fan speed, $N_{1c}$, and is designed to maintain a minimum turbofan LPC stall margin of 10%. The turbofan VAFN is also open-loop scheduled based on $N_{1c}$ while the tailfan VAFN is open-loop scheduled based on corrected tailfan speed, $N_{tc}$. The applied VAFN schedules ensure that the fan modules of the respective subsystems follow an operating line of near optimal efficiency.

Power lever angle (PLA) thrust schedules for the STARC-ABL's turbofan and tailfan subsystem controllers are also derived from the original NPSS model. These schedules apply corrected fan speeds ($N_{1c}$ for the turbofans and $N_{tc}$ for the tailfan) as the thrust feedback parameters scheduled as a function of PLA throttle input. The defined PLA thrust schedules promote coordinated steady-state operation of the turbofan and tailfan subsystems throughout the STARC-ABL's flight envelope (0 to 43k feet altitude and 0 to 0.82 Mach), while maintaining tailfan motor power below its maximum 3500 hp limit.

### 3.3 Integrated Closed-Loop Control Design

The control concept of operations applied in Ref. [19] assumes that the tailfan motor consumes the necessary power from the DC bus to reach its commanded operating state, while the turbofan generators act to hold a target 1000V DC bus voltage. With this assumption, the electrical power system exhibits an aft-to-forward coupling with any changes in the tailfan power demand resulting in a corresponding change in the amount of power the generators extract from the turbofan LP shafts. The amount of power extraction the turbofans can support is dependent on their operating state. Extracting too much power can cause HPC stalls while extracting too little power can cause LPC stalls. This requires coordinated control of the turbofan and tailfan subsystems, especially during transient operation. To address this concern, Ref. [19] applied a single throttle input control strategy where both turbofans receive identical throttle inputs while the tailfan receives a synthesized throttle input calculated as a function of the average fan speed of the two turbofans. This approach maintains coordinated operation between the turbofans and the tailfan during transients while allowing the turbofan fuel control design to be simplified to a single-input single-output linear problem.

The control design process includes the development of proportional plus integral (PI) fan speed setpoint controllers for the tailfan and turbofan. Individual linear setpoint controllers are designed at multiple points spanning the STARC-ABL's operating envelope. To support this control design process, linear state-space models of the following form are extracted from the nonlinear T-MATS model at each design point:

$$\begin{aligned} \dot{x} &= A \cdot \underbrace{(x - x_{trim})}_{\Delta x} + B \cdot \underbrace{(u - u_{trim})}_{\Delta u} \\ \underbrace{(y - y_{trim})}_{\Delta y} &= C \cdot \underbrace{(x - x_{trim})}_{\Delta x} \end{aligned} \qquad (1)$$

with state variable vector, $x$, control input vector, $u$, and sensed measurement vector, $y$. Trim conditions in those same vectors are denoted as $x_{trim}$, $u_{trim}$, and $y_{trim}$, and deviations (Δ's) about those trim conditions are denoted as $\Delta x$, $\Delta u$, and $\Delta y$. Throughout the remainder of this paper the Δ terms are dropped for simplification. Expanding the state-space model vectors and matrices to show individual elements yields Eq. (2). Here, the dynamics of only a single turbofan plus the tailfan are considered. This simplification is possible due to the symmetric operating nature of the two turbofans.

$$\underbrace{\begin{bmatrix}\dot{N}_{2c}\\ \dot{N}_{3c}\\ \dot{N}_{tc}\end{bmatrix}}_{\dot{x}} = \underbrace{\begin{bmatrix}A_{11} & A_{12} & 0\\ A_{21} & A_{22} & 0\\ 0 & 0 & A_{33}\end{bmatrix}}_{A}\underbrace{\begin{bmatrix}N_{2c}\\ N_{3c}\\ N_{tc}\end{bmatrix}}_{x} + \underbrace{\begin{bmatrix}B_{11} & B_{12}\\ B_{21} & 0\\ 0 & B_{32}\end{bmatrix}}_{B}\underbrace{\begin{bmatrix}W_f\\ Q_m\end{bmatrix}}_{u}$$

$$\underbrace{\begin{bmatrix}N_{1c}\\ N_{tc}\end{bmatrix}}_{y} = \underbrace{\begin{bmatrix}C_{11} & 0 & 0\\ 0 & 0 & 1\end{bmatrix}}_{C}\underbrace{\begin{bmatrix}N_{2c}\\ N_{3c}\\ N_{tc}\end{bmatrix}}_{x} \tag{2}$$

The state vector, $x$, includes turbofan corrected LP shaft speed, $N_{2c}$, turbofan corrected core speed, $N_{3c}$, and tailfan corrected speed, $N_{tc}$. The input vector, $u$, includes turbofan fuel flow rate, $W_f$, and tailfan motor torque, $Q_m$. The output vector, $y$, includes $N_{1c}$ and $N_{tc}$. It is noted that within the STARC-ABL's geared turbofan design, $N_{2c}$ and $N_{1c}$ are directly proportional and related by a gear ratio expressed as $N_{2c} = 2.7 \cdot N_{1c}$. The aft-to-forward coupling in the system is reflected in the $B_{12}$ term of the $B$ matrix in Eq. (2). This shows than any change in motor torque $Q_m$ will affect the turbofan's $N_{2c}$ state.

A STARC-ABL closed-loop control architecture can be drawn in block diagram form as illustrated in Fig. 3. Here, the turbofan detail is expanded to show integrator blocks and state-space matrix elements from Eq. (2). Transfer functions reflecting dynamics of the fuel actuator and the tailfan are denoted as $F(s)$ and $G_t(s)$, respectively. Sensor dynamics as well as motor and generator actuator dynamics are excluded from the figure and the control design process as they are assumed to occur on a time scale considerably faster than the turbofan and tailfan shaft dynamics. Also excluded are VBV and VAFN dynamics as they are assumed to operate on-schedule. The setpoint control design process requires design of the two PI controllers, denoted as $K(s)$ for the turbofan fuel controller and $K_m(s)$ for the tailfan motor controller. The gain block, γ, reflects the fractional change in commanded tailfan corrected speed, $N_{tc,cmd}$, based on a change in turbofan corrected fan speed, $N_{1c}$, which is consistent with the choice of constructing a synthesized tailfan PLA based on the average $N_{1c}$ of the two turbofans. This $N_{tc}$:$N_{1c}$ ratio can be thought of as the small perturbation relationship between turbofan and tailfan speeds at a given design point. Consistent with Eq. (2), Motor torque, $Q_m(s)$, is shown as an input feeding directly into both the tailfan and the turbofan.

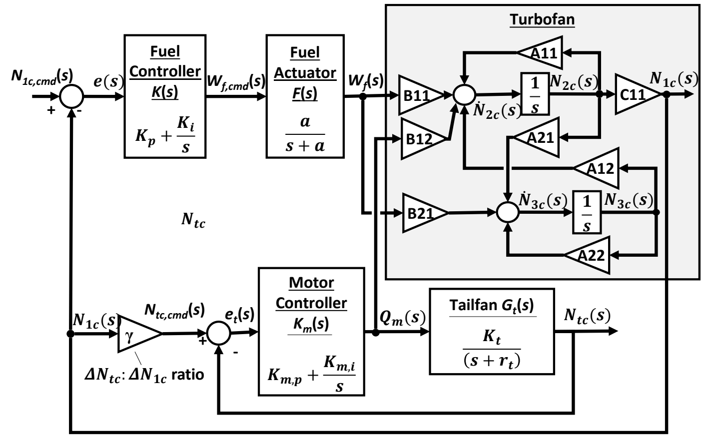


**FIGURE 3:** STARC-ABL CLOSED-LOOP CONTROL ARCHITECTURE.

From Fig. 3, a loop transfer function, $T(s)$, relating $N_{tc,cmd}$ to $Q_m(s)$ can be produced as shown in Eq. (3)

$$T(s) = \frac{Q_m(s)}{N_{tc,cmd}(s)} = \frac{K_m(s)}{I + K_m(s)G_t(s)} \tag{3}$$

As detailed in Ref. [19], $T(s)$ can be combined with other elements of Fig. 3 to produce the following single-input single-output transfer function relating turbofan fuel flow rate input, $W_f$, to turbofan $N_{1c}$ output:

$$\frac{N_{1c}(s)}{W_f(s)} = \frac{B_{11}C_{11}\left(s + \frac{A_{12}B_{21}}{B_{11}} - A_{22}\right)}{(s - A_{11})(s - A_{22}) - A_{12}A_{21} - C_{11}\gamma T(s)B_{12}(s - A_{22})} \tag{4}$$

Tailfan power extraction coupling effects are captured in the $C_{11}\gamma T(s)B_{12}(s - A_{22})$ portion of the Eq. (4) denominator.

In addition to the setpoint controller, the baseline STARC-ABL fuel control system also includes acceleration and deceleration schedules based on a fan speed derivative, $\dot{N}_{1c}$, plus a minimum HPC exit static pressure (*Ps3*) limiter. The tailfan motor controller includes its setpoint controller plus a maximum horsepower limiter. Setpoint, transient, and limit controllers are designed at multiple operating points spanning the STARC-ABL operating envelope. They are then combined in a piecewise linear gain scheduling fashion to provide nonlinear full operating envelope control functionality [22]. Throughout a flight, the control system automatically switches its operating mode between setpoint, transient, and limit controllers by applying conventional maximum-minimum mode selection logic to determine which control regulator is active at any instant in time [22,23]. Smooth transition between the controllers is managed by integrator windup protection-based bumpless transfer logic.

## 4. SUBSYSTEM FAILURE MODES AND EFFECTS

A high-level assessment of the STARC-ABL's subsystem failure modes and their effects was conducted in Ref. [6] and is summarized in Fig. 4. Here, only abrupt complete functional failures of a single subsystem are considered as opposed to failures resulting in a partial loss of functionality or failures occurring simultaneously in multiple subsystems. The failures are listed in the Fig. 4 columns and include a failure of turbofan 1, turbofan 2, power string 1, power string 2, or the tailfan. The rows reflect the coupled effects of each failure on other subsystems when the system is operating under the original baseline control design.

| Coupled Failure Effects on Other Subsystems | Failed Subsystem: Turbofan 1 Failed | Turbofan 2 Failed | Power String 1 Failed | Power String 2 Failed | Tailfan Failed |
|---|---|---|---|---|---|
| Turbofan 1 | *Failed* | *Increased HPX* | *No HPX* | *Increased HPX* | *No HPX* |
| Turbofan 2 | *Increased HPX* | *Failed* | *Increased HPX* | *No HPX* | *No HPX* |
| Power String 1 | *No Electric Power* | *Increased Electric Power* | *Failed* | *Increased Electric Power* | *No Electric Power* |
| Power String 2 | *Increased Electric Power* | *No Electric Power* | *Increased Electric Power* | *Failed* | *No Electric Power* |
| Tailfan | *Reduced Electric Power* | *Reduced Electric Power* | *Reduced Electric Power* | *Reduced Electric Power* | *Failed* |

**Figure 4**: STARC-ABL FAILURE MODES AND EFFECTS.

The baseline STARC-ABL configuration and control concept can lead to either increased or no turbofan horsepower extraction (HPX) upon subsystem failures. Of particular concern is the failure of either a turbofan or a power string. Under such failures, the tailfan speed controller would attempt to draw 100% of the necessary power to hold the commanded tailfan speed setpoint from the remaining nominally operating turbofan and its power string. This could happen very rapidly, leading to a compressor stall and shutdown of the remaining healthy engine—a potentially catastrophic event. Avoidance of this scenario would require an extremely fast responding fault detection and accommodation strategy, which may not be possible at the time-scales of gas turbine engine controls. To alleviate this concern, this study partitions the STARC-ABL DC power bus and the tailfan motor into two separate parallel power strings. Each string is supplied power by an individual turbofan generator and contributes 50% of the total electrical power delivered to the tailfan. This revised configuration is shown in Fig. 5. In contrast to Fig. 2 which contained a single inverter driving the tailfan motor, Fig. 5 shows the motor equipped with two redundant field windings each energized by a separate power string. In the event of a single turbofan or power string failure, the remaining healthy turbofan and power string can still provide electrical power to the tailfan. This allows the tailfan to continue to operate in the presence of such failures, albeit at a reduced maximum thrust level compared to the nominal design. In addition to the added power string redundancy, it was assumed that each turbofan generator and power string could be operated at 125% of its maximum continuous power level for up to five minutes. This five-minute maximum power operational time is consistent with typical turbofan maximum thrust operating limits [24] and offers slightly increased thrust output under contingency operating scenarios.

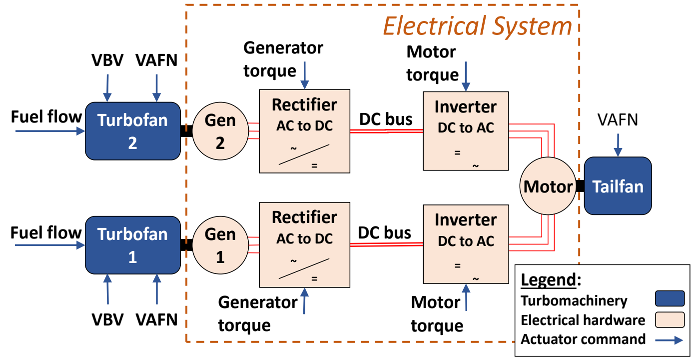


**Figure 5:** REVISED STARC-ABL PROPULSION SYSTEM.

## 5. DETECTION LOGIC AND REVERSIONARY CONTROL MODES FOR FAILURE MITIGATION

Given the revised STARC-ABL propulsion architecture of Fig. 5, steps were taken to develop associated failure detection and reversionary control logic to mitigate potential failure events. This assumed that each turbofan control system is designed to operate either nominally (Mode 0) or in a reversionary control mode including no HPX (Mode 1) or increased HPX (Mode 2). Similarly, the tailfan control system could operate either nominally (Mode 0) or a reversionary control mode of reduced available power (Mode 1). The specific control modes that are activated upon the detection of any individual subsystem failure are shown in Fig. 6. Here, the columns denote the identified failed subsystem, and the rows denote the corresponding control mode activated for the turbofan and tailfan subsystems.

| | Nominal | Failed Subsystem | | | | |
|---|---|---|---|---|---|---|
| | Nominal | Turbofan 1 Failed | Turbofan 2 Failed | Power System 1 Failed | Power System 2 Failed | Tailfan Failed |
| Turbofan 1 | *Mode 0* | *N/A* | *Mode 2* | *Mode 1* | *Mode 2* | *Mode 1* |
| Turbofan 2 | *Mode 0* | *Mode 2* | *N/A* | *Mode 2* | *Mode 1* | *Mode 1* |
| Tailfan | *Mode 0* | *Mode 1* | *Mode 1* | *Mode 1* | *Mode 1* | *N/A* |

**Figure 6:** NOMINAL AND REVERSIONARY CONTROL MODES FOR STARC-ABL SUBSYSTEMS.

### 5.1 Failure Detection and Control Mode Activation Logic

The reversionary control system provides accurate and timely diagnosis of subsystem failures and system-level coordination of the control modes activated within the subsystems. In this study, the logic applied to activate the appropriate control mode for an individual turbofan's control system is shown in Eq. (5). By default, the system begins in Mode 0 operating under nominal baseline control. The control system is updated on a 15 ms control cycle interval. During each control cycle, detection logic assesses the sensed HPX load that the generator applies to the LP shaft of the turbofan. If the HPX load drops below 100 hp and persists below that threshold for three control cycle counts (45 ms), the turbofan's control system will automatically switch to Mode 1—the reversionary control mode associated with no generator HPX taken from the turbofan's LP shaft (see Fig. 6). This logic will cause the turbofan controller to transition to Mode 1 if either its attached power string or the tailfan experiences a failure. The three control cycle count persistency is added to help avoid nuisance false alarms caused due to measurement noise. Upon transition to Mode 1, the generator in the power string attached to the turbofan is disabled from further use. In addition to monitoring generator HPX load, the logic also monitors the control mode of the companion turbofan installed on the opposite wing. If a turbofan's control system is operating in Mode 0 and the companion turbofan's control system is persistently operating in Mode 1 for 10 control cycle counts (150 ms) the turbofan's control system will switch to Mode 2—the control mode associated with extra generator HPX. This switch to Mode 2 will permit HPX loads up to 125% of nominal while adhering to a maximum turbine inlet temperature limit. The 10 cycle persistency requirement for an engine's control system to transition to Mode 2 is intentionally longer than the three cycle persistency requirement to transition to Mode 1 to allow for the possibility of a tailfan failure. Upon a tailfan failure, both engine controllers should ultimately transition to Mode 1 (see Fig. 6). However, this transition may not occur at the same time due to signal measurement noise. The 10 cycle persistency guards against an engine controller erroneously transitioning from Mode 0 to Mode 2 upon a tailfan failure.

$$\begin{array}{c}\text{Turbofan}\\ \text{Control}\\ \text{Mode}\end{array} = \begin{cases} \text{Mode 0, nominal default starting Mode} \\ \text{Mode 1, if Generator HPX < 100hp for three consecutive cycle counts OR Turbofan shutdown OR Tailfan shutdown occurs} \\ \text{Mode 2, if Turbofan Control Mode = Mode 0 AND companion Turbofan Control Mode = Mode 1 for 10 consecutive cycle counts} \end{cases} \tag{5}$$

Reversionary control mode activation logic for the tailfan controller is shown in Eq. (6). The tailfan controller also begins in a nominal control Mode 0. Activation logic monitors the current active control mode of both turbofans. If either turbofan control system switches out of its nominal control Mode 0 into Mode 1, the tailfan controller immediately transitions to its control Mode 1—operation under reduced maximum available power. If the companion Turbofan control system later transitions to Mode 2, the tailfan controller will remain in Mode 1 but the maximum power limit of the power string attached to the turbofan operating in Mode 2 will increase to 125%.

$$\begin{array}{c}\text{Tailfan}\\ \text{Control}\\ \text{Mode}\end{array} = \begin{cases} \text{Mode 0, nominal default starting Mode} \\ \text{Mode 1, if Turbofan Control Mode = Mode 1 AND companion Turbofan Control Mode = Mode 0} \end{cases} \tag{6}$$

The reversionary control logic assumes that if a subsystem failure is detected, the power string components associated with that failed subsystem will be disabled and remain inoperable unless the failed subsystem undergoes a successful in-flight restart. Given this assumption, all control mode transitions under failure conditions are unidirectional. The turbofan controller can transition directly from its Mode 0 to either Mode 1 or Mode 2. Transitions from Mode 2 to Mode 1 are also permissible. However, once operating in Mode 1, which results in the attached power string being disabled, the system cannot transition back to Mode 0 or Mode 2. Similarly, if the tailfan controller transitions to Mode 1, it cannot transition back to Mode 0. The current implementation of the reversionary control design does not yet include logic to facilitate a transition from a reversionary control mode back to nominal. Follow-on work to add this functionality is recommended.

### 5.2 Reversionary Control Mode Design

Figure 7 shows STARC-ABL linear state-space models and trim conditions to illustrate the variation in system dynamics under different subsystem failure scenarios and control modes. For this example, all linear state-space models are extracted from the nonlinear T-MATS STARC-ABL model at the sea level static (SLS) and $N_{1c}$ = 4200 rpm operating point. The resulting linear models take the form of the state-space model previously introduced in Eqs. (1) and (2). Figure 7a shows the state-space model when the system is operating failure free with all subsystem controllers in their nominal control Mode 0. Figure 7b shows the state-space model for an individual turbofan operating in control Mode 1 with a failure either in its attached power string or the tailfan. Tailfan loading and dynamics are omitted from Fig. 7b. Figure 7c shows the state-space model for an individual turbofan operating in its control Mode 2 and the tailfan in its control Mode 1 with a failure in the opposite engine or power string. Comparing the trim vectors and state-space matrix elements illustrates the variation in steady-state operation and system dynamics that is occurring across these three scenarios. To facilitate control design, linear state-space models spanning the STARC-ABL's operating envelope are produced for each of the scenarios. These models are then used to design a complete control system for the STARC-ABL, including the nominal baseline control and the reversionary control modes.

As shown in Fig. 6, any turbofan or power string failure will result in the tailfan operating in its reversionary control Mode 1. In this control mode, all tailfan motor power is supplied by a single turbofan and its attached power string. This requires a revised tailfan PLA to $N_{tc}$ thrust schedule that is compatible with the power production capabilities of a single turbofan and its power string. A comparison of the nominal (Mode 0) and reversionary (Mode 1) PLA to $N_{tc}$ schedules for the tailfan at SLS conditions is provided in Fig. 8 along with resultant effects on other system parameters. The PLA to $N_{tc}$ schedule comparison, which is provided in Fig. 8a, shows the tailfan operating at a lower speed in control Mode 1. The total tailfan

$$x_{trim} = \begin{bmatrix} N_{2c} \\ N_{3c} \\ N_{tc} \end{bmatrix} = \begin{bmatrix} 11340 \\ 22430 \\ 2178 \end{bmatrix} \qquad A = \begin{bmatrix} -2.478 & 2.001 & 0 \\ 2.901 & -15.516 & 0 \\ 0 & 0 & -3.103 \end{bmatrix}$$

$$u_{trim} = \begin{bmatrix} W_f \\ Q_m \end{bmatrix} = \begin{bmatrix} 4388 \\ 8440 \end{bmatrix} \qquad B = \begin{bmatrix} 1.466 & -0.165 \\ 6.282 & 0 \\ 0 & 0.398 \end{bmatrix}$$

$$y_{trim} = \begin{bmatrix} N_{1c} \\ N_{tc} \end{bmatrix} = \begin{bmatrix} 4200 \\ 2178 \end{bmatrix} \qquad C = \begin{bmatrix} 0.370 & 0 \\ 0 & 1 \end{bmatrix}$$

a) Nominal (Turbofan Mode 0 & Tailfan Mode 0)

$$x_{trim} = \begin{bmatrix} N_{2c} \\ N_{3c} \\ N_{tc} \end{bmatrix} = \begin{bmatrix} 11340 \\ 22214 \\ - \end{bmatrix} \qquad A = \begin{bmatrix} -3.207 & 3.333 & - \\ 5.053 & -20.532 & - \\ - & - & - \end{bmatrix}$$

$$u_{trim} = \begin{bmatrix} W_f \\ Q_m \end{bmatrix} = \begin{bmatrix} 3798 \\ - \end{bmatrix} \qquad B = \begin{bmatrix} 1.498 & - \\ 6.737 & - \\ - & - \end{bmatrix}$$

$$y_{trim} = \begin{bmatrix} N_{1c} \\ N_{tc} \end{bmatrix} = \begin{bmatrix} 4200 \\ - \end{bmatrix} \qquad C = \begin{bmatrix} 0.370 & 0 \\ 0 & 1 \end{bmatrix}$$

b) Attached Power String or Tailfan Failure (Turbofan Mode 1)

$$x_{trim} = \begin{bmatrix} N_{2c} \\ N_{3c} \\ N_{tc} \end{bmatrix} = \begin{bmatrix} 11340 \\ 22520 \\ 1866 \end{bmatrix} \qquad A = \begin{bmatrix} -2.082 & 1.075 & 0 \\ 0.7119 & -10.547 & 0 \\ 0 & 0 & -2.551 \end{bmatrix}$$

$$u_{trim} = \begin{bmatrix} W_f \\ Q_m \end{bmatrix} = \begin{bmatrix} 4551 \\ 6165 \end{bmatrix} \qquad B = \begin{bmatrix} 1.470 & -0.282 \\ 6.179 & 0 \\ 0 & 0.398 \end{bmatrix}$$

$$y_{trim} = \begin{bmatrix} N_{1c} \\ N_{tc} \end{bmatrix} = \begin{bmatrix} 4200 \\ 1866 \end{bmatrix} \qquad C = \begin{bmatrix} 0.370 & 0 \\ 0 & 1 \end{bmatrix}$$

c) Opposite Turbofan or Opposite Power String Failure (Turbofan Mode 2 & Tailfan Mode 1)

**Figure 7:** COMPARISON OF STATE-SPACE MODELS FOR NOMINAL AND REVERSIONARY CONTROL MODES (SEA LEVEL STATIC, 4200 RPM N1C OPERATING POINT).

motor power contributed by the combination of power string 1 and power string 2 (see Fig. 5) is shown in Fig. 8b. Under Mode 0 operation, up to 3500 hp of total motor power can be delivered to the tailfan with each string contributing 50% (1750 hp). Under Mode 1 operation, the maximum total motor power is reduced to 2188 hp with all power provided by a single power string attached to one of the motor's two field windings. Turbofan generator LP shaft HPX and the ratio of generator LP shaft HPX to low pressure turbine hp input (denoted HPX ratio) are shown in Fig. 8c and Fig. 8d, respectively, for turbofans operating in control Modes 0, 1, or 2. Under nominal conditions (Mode 0) a maximum generator LP shaft HPX level of 1942 hp is reached when total tailfan motor power is at its 3500 hp operating limit. Under failure conditions, the LP shaft HPX of the turbofan operating in control Mode 2 increases to 2428 hp while the companion engine's LP shaft HPX drops to 0 hp and its controller operates in Mode 1. Figure 8d shows an elevated LP shaft HPX ratio for Mode 2 compared to Mode 0 at the higher PLA settings when the motor power limit is encountered. Once PLA is reduced to the point where the turbofan LP HPX ratio of 28% is encountered, that ratio is maintained through idle.

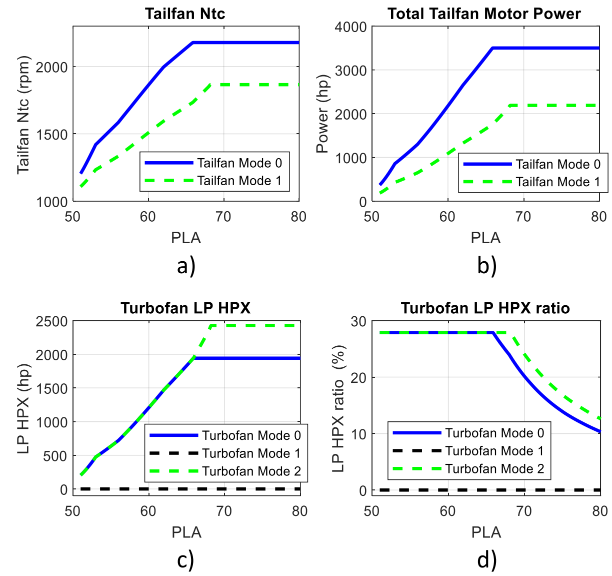


**Figure 8:** COMPARISON OF NOMINAL AND REVERSIONARY CONTROL THRUST SCHEDULE EFFECTS (SLS CONDITION).

Turbofan VBV actuator position is open-loop scheduled as a function of $N_{1c}$ to maintain a minimum steady-state LPC stall margin of 10%. As LPC stall margin is dependent on the amount of generator HPX demand placed on a turbofan's LP shaft, modified turbofan VBV schedules are necessary for the reversionary control modes. VBV schedules and LPC stall margins for all control modes are shown in Fig. 9 for the SLS condition. The VBV is fully closed and LPC stall margin is greater than 10% at high $N_{1c}$ speeds in all modes. The VBV remains closed as $N_{1c}$ is reduced until LPC stall margin reaches 10%. At this point, the VBV schedule transitions from closed to opening to maintain a 10% LPC stall margin. For reversionary control Mode 1 (the failure case with no LP shaft HPX), the point where the VBV transitions from closed to opening occurs at a higher $N_{1c}$ speed. The VBV schedules for Mode 0 and Mode 2

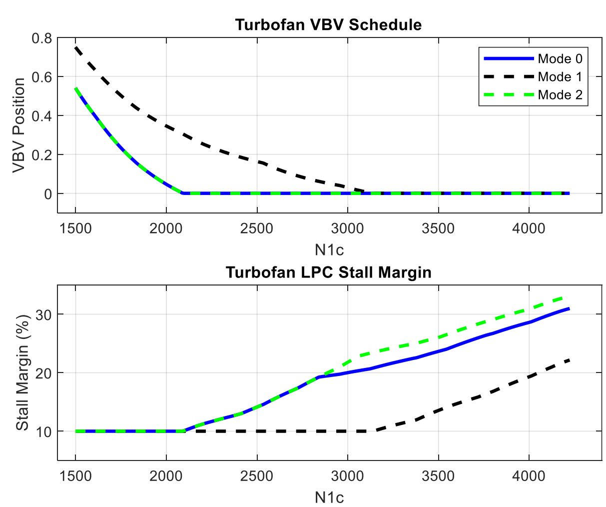


**Figure 9:** NOMINAL AND REVERSIONARY CONTROL VBV SCHEDULING AND LPC STALL MARGIN (SLS CONDITION).

are identical at this condition as both control modes are operating on the 28% LP shaft HPX ratio schedule at the $N_{1c}$ speed when the 10% LPC stall margin is encountered.

All turbofan control modes apply identical $\dot{N}_{1c}$ acceleration and deceleration schedules. This allows similar $N_{1c}$ transient response between the two turbofans to be maintained under nominal operation or during failure scenarios with one turbofan in control Mode 1 and the opposite turbofan in control Mode 2.

The design process for each control mode was performed over a range of operating conditions and combined with the failure detection and control mode transition logic to provide full flight envelope functionality. To promote stability, the PI control loops within all control modes were designed to provide a minimum of 8 dB gain margin and 55 degrees phase margin. This, in combination with the included integrator windup protection logic, was found to promote smooth transition between the controllers.

## 6. REAL-TIME HARDWARE IN THE LOOP TEST

To evaluate the performance of the newly developed STARC-ABL reversionary control logic, a HIL test was performed at the Hybrid Propulsion Emulation Rig (HyPER) located at the NASA Glenn Research Center in Cleveland, Ohio. The HyPER electrical hardware operates at power levels of approximately 100 kW, which is significantly less than the 2.6 MW STARC-ABL electrical system. As such, the HyPER test is set up as a "subscale" HIL test of the STARC-ABL power system. HyPER electrical hardware includes shaft-mounted electric machines, power converters, power supplies, power distribution cables, and an energy storage device, which can be configured to represent a variety of EAP architectures [25]. It also includes an integrated real-time computer system that hosts EAP control software and turbomachinery simulations. This enables the electrical system and rotating shafts of EAP designs to be implemented in actual hardware and integrated with turbomachinery simulations and system-level control logic implemented in software. In this form, HyPER provides a HIL test configuration enabling the initial development and evaluation of EAP control technology in an environment that includes actual electrical system hardware.

### 6.1 Test Configuration

The HyPER STARC-ABL controls test configuration is shown in Fig. 10. Here, a full-scale nonlinear simulation of the STARC-ABL turbomachinery and the control software are coded as a real-time application and implemented in a dSPACE SCALEXIO real-time computing system while a subscale version of the turbofan 1 LP shaft, the tailfan shaft, and their attached electrical power string are implemented in hardware. The hardware configuration includes two rotating shafts, each with an attached pair of 66 kW electric machines and inverters. The inverters are configured to accept torque command inputs and supply speed feedback measurements to the dSPACE SCALEXIO. Two 100 kW bi-directional power supplies provide power to the inverters over 350 V DC power buses. Each physical shaft enables the emulation of an electrified turbomachinery shaft with one of the attached electric machines emulating the shaft dynamics and torque load while the other electric machine acts as a motor or generator.

A slight limitation for this test is that HyPER only contains two rotating shafts. Ideally, a three-shaft configuration is preferred for emulating all three electrified shafts of the STARC-ABL (e.g., turbofan 1 LP shaft and generator, turbofan 2 LP shaft and generator, and tailfan shaft and motor). Such a three-shaft configuration was used for previous testing of the STARC-ABL baseline control design in another NASA Glenn facility [19,26]. Given the HyPER two-shaft limitation, an implementation decision was made to only emulate power string 1 in actual hardware, while power string 2 was implemented entirely in simulation. For power string 1 emulation, one of the two available shafts was used for emulating the LP shaft of turbofan 1 and its generator. The remaining shaft was used for emulating the portion of the tailfan motor energized by power string 1 and the loading placed upon it by the tailfan. Overall, the two-shaft implementation was a minor impact as the symmetry within the system still allowed all subsystem failures and reversionary

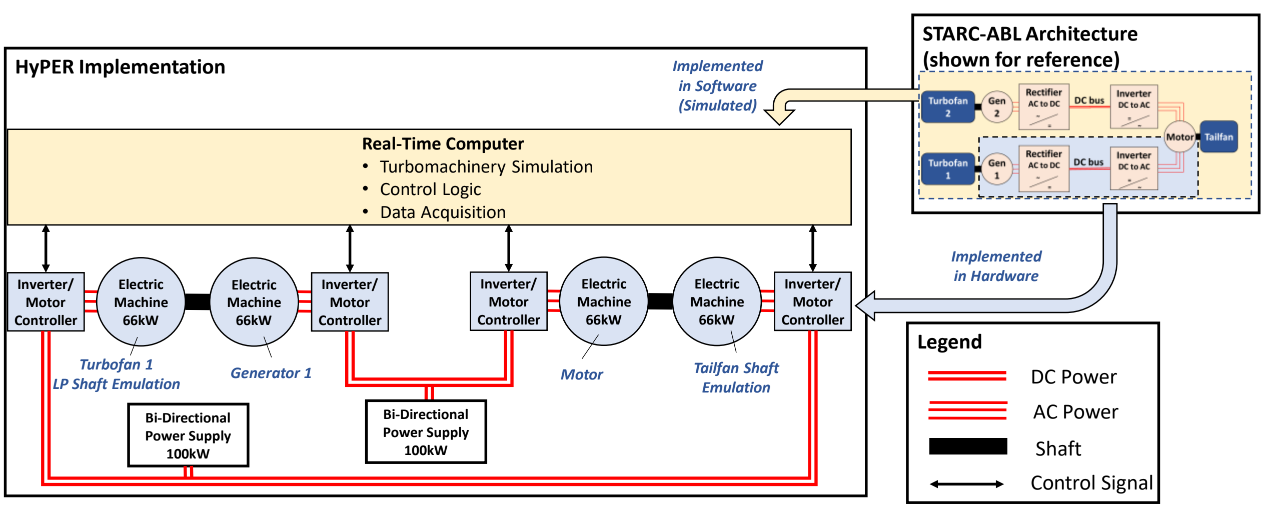


**Figure 10:** HYPER STARC-ABL REVERSIONARY CONTROLS TEST CONFIGURATION.

control modes to be tested. During testing, subsystem failures were emulated through logic included in the real-time computer that allowed electric machine torque commands to be abruptly stepped to zero. In this manner, the failure of either power string could be emulated by simultaneously stepping both its generator and motor commanded torque values to zero. This action eliminated all LP shaft HPX from the associated turbofan as well as all electrical power transferred to the associated tailfan motor winding. Using this strategy to emulate the failure of a single power string enabled evaluation of failure scenarios that resulted in the attached turbofan operating in control Mode 1, the companion turbofan in control Mode 2, and the tailfan in its control Mode 1. Alternatively, the same strategy could be applied to simultaneously fail both power strings, which would emulate a tailfan failure with both turbofans operating in control Mode 1.

To allow the STARC-ABL reversionary control design to be tested in HyPER without modification, several differences between the full-scale STARC-ABL and subscale HyPER implementation are accounted for. These include differences in electric machine power levels, rated operating speeds, rotational shaft inertia, and viscous damping. To address these inconsistencies, an innovative adaptive sliding mode impedance controller with scaling (ASMICS) algorithm is applied [27]. This algorithm scales the torque and speed signals passed between the real-time computer and the electrical hardware. It also adjusts the torque commands supplied to the electric machines tasked with emulating turbomachinery shaft dynamics, which allows those machines to accurately represent specified subscale inertias and loads. With the inclusion of this technology, the evaluated reversionary control system perceived that it was controlling an actual full-scale STARC-ABL propulsion system.

The real-time application implemented on the dSPACE SCALEXIO provided integrated multifunctional capability [26]. This included real-time execution of the STARC-ABL nonlinear simulation, ASMICS, inverter communication, data acquisition, graphical user interface display drivers, plus the STARC-ABL reversionary control logic under test. All logic ran at a 15 ms control cycle update interval without issue.

### 6.2 Test Results

HyPER testing enabled comparison of the performance of the original baseline STARC-ABL control design presented in Ref. [19] to the newly developed reversionary control design presented in this paper. It included a variety of nominal and failed operating scenarios conducted over multiple flight conditions. Figure 11a shows baseline control results from PLA burst/chop testing conducted at the SLS condition. Here, transient control performance is evaluated by introducing a PLA burst from idle to maximum throttle at time 40 s followed by a PLA chop from maximum throttle to idle at time 70 s. Figure 11a includes results from two separate tests—the first test performed with a power string 1 failure introduced at time 10 s and the second test with all subsystems performing nominally (failure-free). The top two rows of subplots show turbofan data with the thick blue and red lines reflecting the failure test case response of turbofan 1 and turbofan 2, respectively, while the thin yellow line reflects the nominal test case response of just turbofan 1. Turbofan 2 data are not shown for the nominal case as it closely matches that of turbofan 1 due to the symmetric nature of the STARC-ABL under nominal operating conditions. The bottom row of subplots shows tailfan data from the same two test cases with the thick blue lines reflecting the failure test case data and the thin yellow line reflecting nominal test case data. For the failure test case, a departure in the operation of the two turbofans is immediately apparent upon failure occurrence as turbofan 2 begins providing all power delivered to the tailfan. The system continues to operate post-failure up until the PLA chop is introduced. Then, during the ensuing deceleration, a turbofan 1 LPC stall at time 73 s occurs and the HyPER test is halted.

Figure 11b shows results from the same test scenarios with the newly developed reversionary control logic enabled. In this case, the failure is promptly detected, and the subsystem controllers automatically switch to their appropriate reversionary control modes—turbofan 1 in Mode 1, turbofan 2 in Mode 2, and the tailfan in Mode 1. This applies revised turbofan VBV schedules, which allows the test to run to completion without encountering a turbofan 1 LPC stall. The reversionary control logic also applies an updated tailfan PLA-to-$N_{tc}$ schedule that allows power string 2 to operate up to 125% power levels. This enables a 16% increase in the maximum tailfan net thrust output compared to the baseline control design.

Figure 12 shows analogous results for PLA burst/chop testing performed at a 37k feet 0.78 Mach cruise condition, this time with a failure inserted in power string 2. Baseline control test results are shown in Fig. 12a. Here, it is observed that turbofan 1 experiences an HPC stall at approximately 44 s during the initial acceleration transient. This stall event is caused by an excessive generator HPX load placed upon the LP shaft of turbofan 1. If the resulting compressor stall leads to a turbofan 1 shutdown, all electrical power delivered to power string 1 will be lost. A loss of power string 1, coupled with the original power string 2 failure given in this example, will eliminate all electrical power delivered to the tailfan. This will result in a tailfan shutdown. If these cascading failures occur, the only remaining source of vehicle thrust will be turbofan 2 operating with no generator LP shaft HPX—a condition that places a turbofan at elevated risk for experiencing LPC stalls upon deceleration as was shown in Fig. 11a. The loss of turbofan 2 in this case would result in a catastrophic total vehicle loss of thrust.

Figure 12b shows results for this same 37k feet 0.78 Mach cruise condition with the reversionary control enabled. In this case, the failure is properly detected, the subsystem controllers automatically enter their appropriate reversionary control modes to enable failure mitigation, and the acceleration and deceleration transients occur without issue. Here, a turbofan 1 HPC stall event during the acceleration is avoided due to the reversionary control's updated PLA-to-$N_{tc}$ schedule that places a lower LP shaft HPX load on turbofan 1.

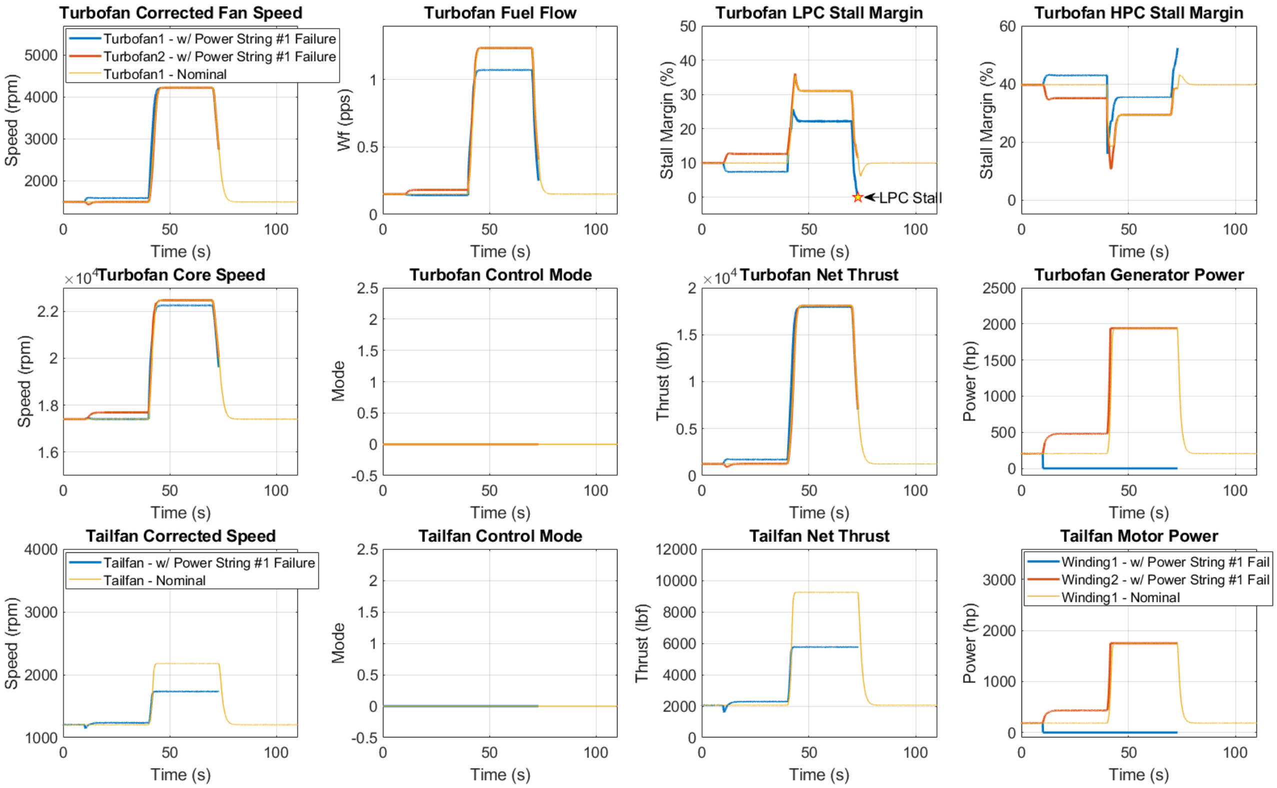


a) Baseline Control

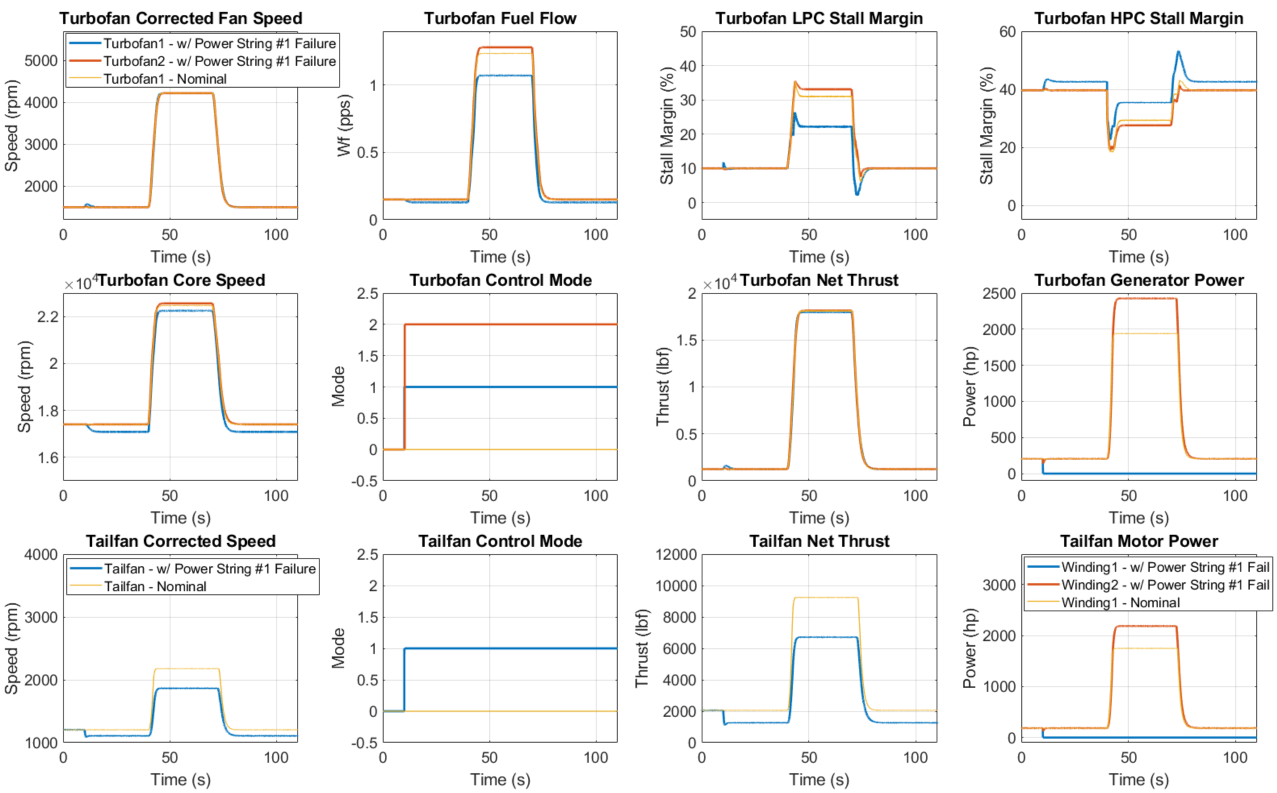


b) Reversionary Control

**Figure 11:** PLA BURST / CHOP RESULTS AT SLS CONDITION WITH POWER STRING #1 FAILURE.

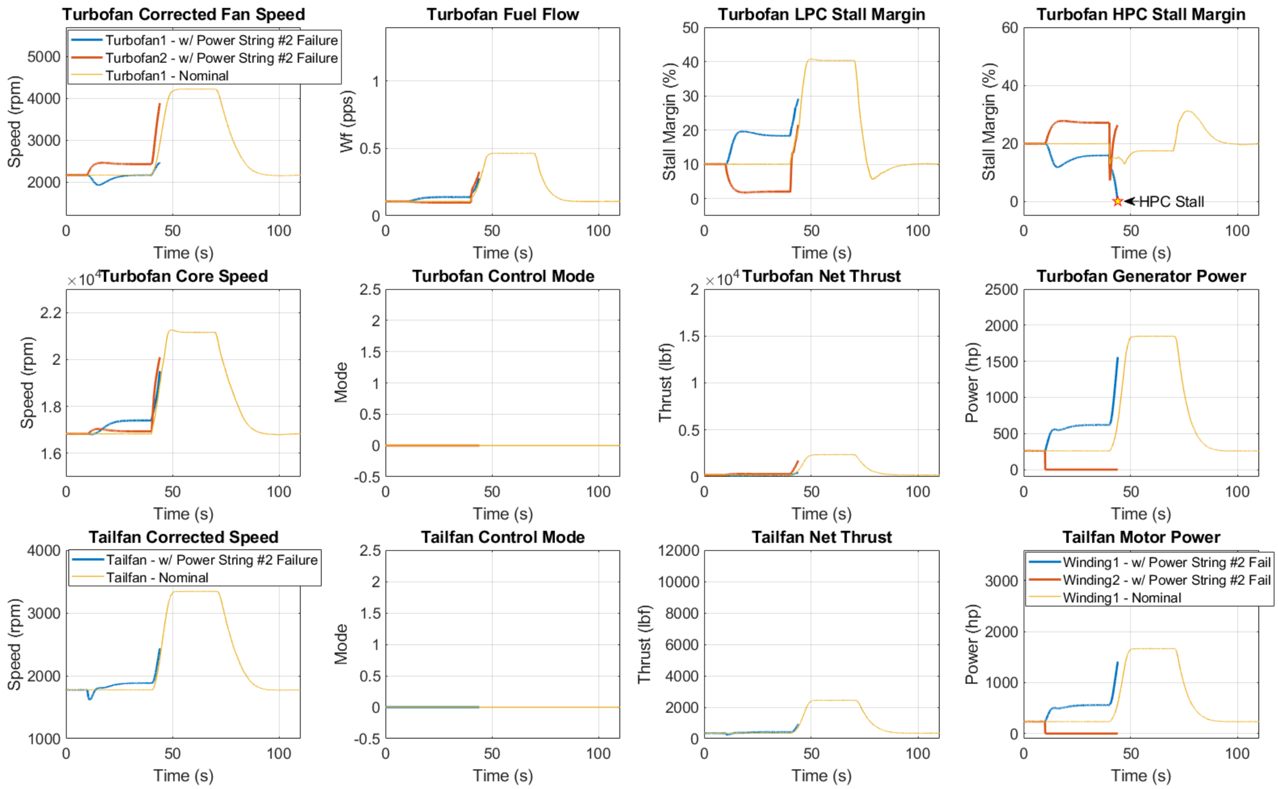


a) Baseline Control

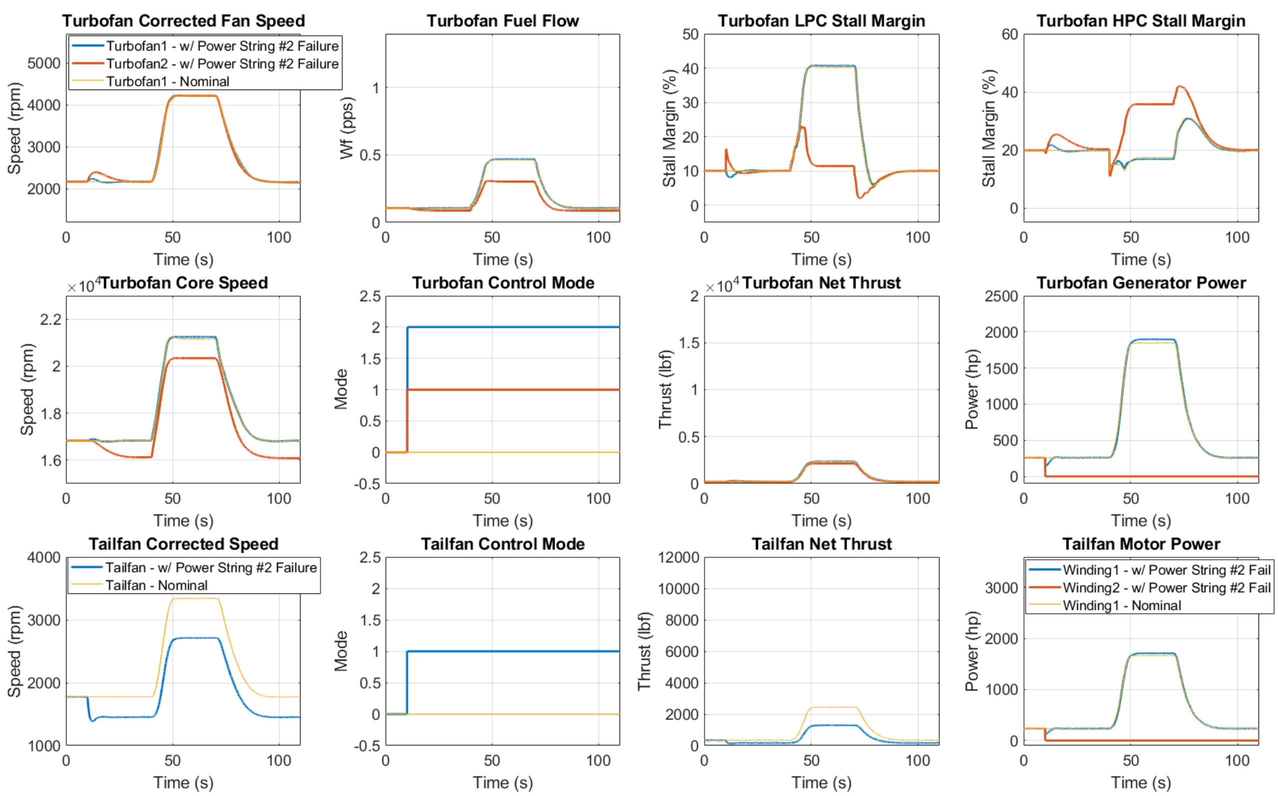


b) Reversionary Control

**Figure 12:** PLA BURST / CHOP RESULTS AT CRUISE CONDITION WITH POWER STRING #2 FAILURE.

To further assess the robustness of the reversionary control logic, HyPER testing also included scenarios where failures were inserted during acceleration and deceleration transients. Figure 13 shows results for a power string 1 failure during an idle to maximum PLA acceleration transient at SLS conditions. Here, the transient starts at time 40 s and a failure occurs at time 42.1 s. The failure induces slight fluctuations in the system variables, but failure detection and reversionary control activation occur in adequate time to enable the transient to proceed without issue. Figure 14 shows analogous results for a power string 2 failure during a maximum to idle PLA deceleration transient performed at the 37k feet 0.78 Mach condition. Once again, failure detection and reversionary control activation occur in ample time to enable the successful completion of the transient without issue.

The STARC-ABL's maximum net thrust output under both nominal and reversionary control operation was assessed throughout the vehicle's operating envelope. Results for the SLS and 37k feet 0.78 Mach cruise conditions are shown in Table 1 and Table 2, respectively. Each table includes the percent of nominal maximum total vehicle thrust output of the vehicle and the subsystems when operating nominally and under failure conditions. At SLS the maximum total vehicle thrust output is 45,433 lbf. For the cruise condition, it is 7,171 lbf. In all failure cases the total vehicle net thrust remained above 50% of the nominal (failure free) operating condition. As expected, turbofan failures resulted in the largest thrust loss. In these cases, the total vehicle net thrust is 54.7% of nominal for the SLS condition and 51.1% of nominal for the cruise condition. For individual power system failures, the resulting total vehicle net thrust is 94.2% of nominal at SLS and 81.0% of nominal at cruise. For tailfan failure, the total vehicle net thrust was 79.0% of nominal at SLS and 59.7% of nominal at cruise.

**Table 1**. PERCENT MAXIMUM NET THRUST AT SLS

| | Failed Subsystem | | | | | |
|---|---|---|---|---|---|---|
| Thrust source | No Failure | Turbo-fan 1 | Turbo-fan 2 | Power Str. #1 | Power Str. #2 | Tailfan |
| Turbofan1 | 39.8% | 0% | 39.9% | 39.5% | 39.9% | 39.5% |
| Turbofan2 | 39.8% | 39.9% | 0% | 39.9% | 39.5% | 39.5% |
| Tailfan | 20.3% | 14.8% | 14.8% | 14.8% | 14.8% | 0% |
| Vehicle Thrust | 100% | 54.7% | 54.7% | 94.2% | 94.2% | 79.0% |

**Table 2.** PERCENT MAXIMUM NET THRUST AT CRUISE

| | Failed Subsystem | | | | | |
|---|---|---|---|---|---|---|
| Thrust source | No Failure | Turbo-fan 1 | Turbo-fan 2 | Power Str. #1 | Power Str. #2 | Tailfan |
| Turbofan1 | 33.0% | 0.0% | 33.1% | 29.8% | 33.1% | 29.8% |
| Turbofan2 | 33.0% | 33.1% | 0.0% | 33.1% | 29.8% | 29.8% |
| Tailfan | 34.0% | 18.0% | 18.0% | 18.0% | 18.0% | 0.0% |
| Vehicle Thrust | 100% | 51.1% | 51.1% | 81.0% | 81.0% | 59.7% |

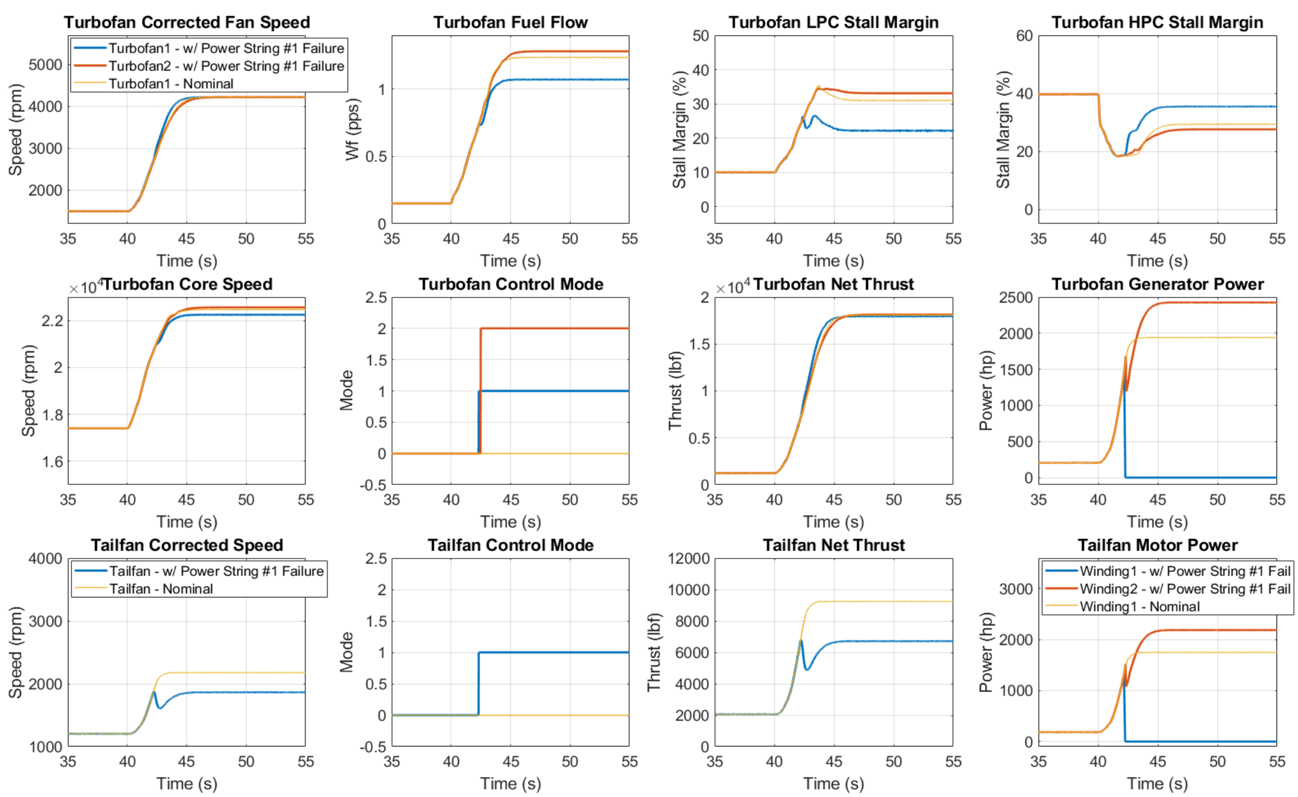


**Figure 13:** POWER STRING #1 FAILURE DURING ACCELERATION TRANSIENT AT SLS CONDITION (REVERSIONARY CONTROL).

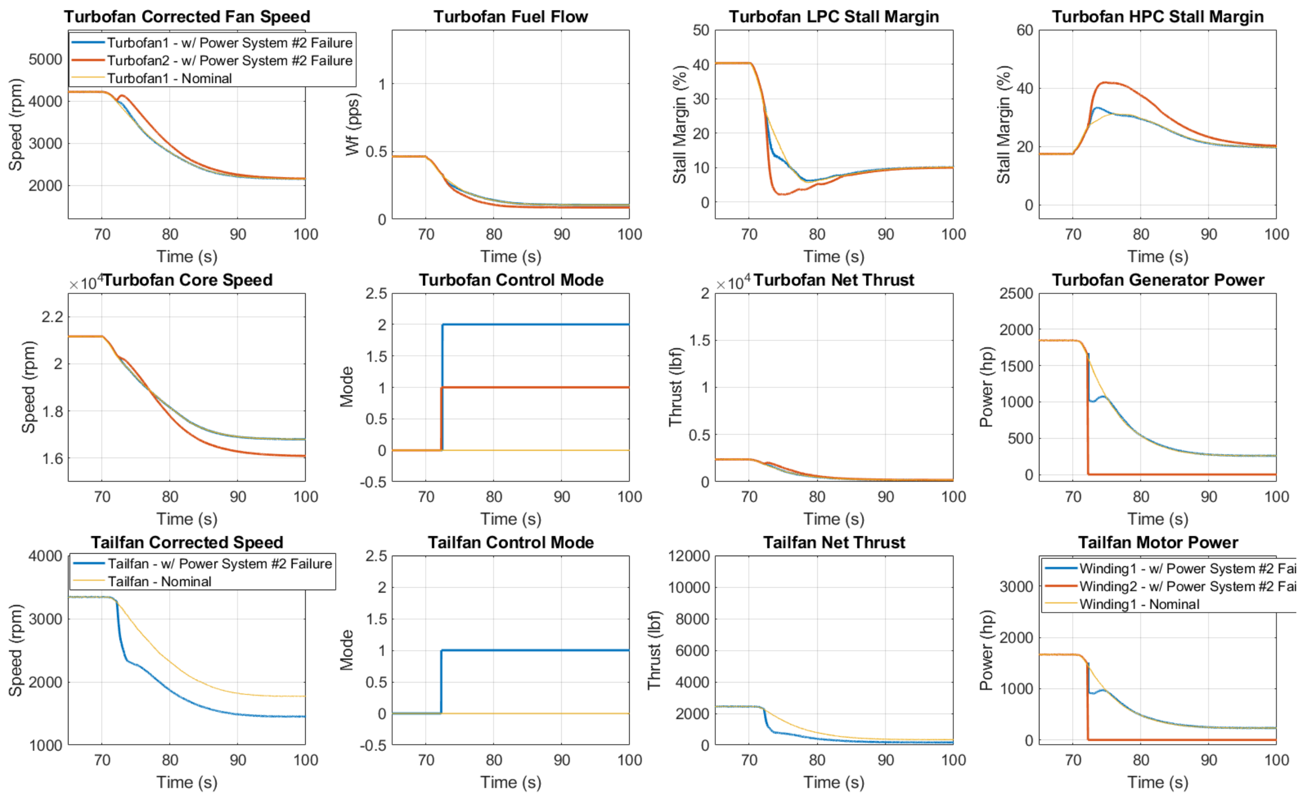


**Figure 14:** POWER STRING #2 FAILURE DURING DECEL TRANSIENT AT CRUISE CONDITION (REVERSIONARY CONTROL).

## 7. DISCUSSION

The reversionary control study presented in this paper illustrates several of the challenges and potential solutions associated with failure mitigation in EAP architectures. However, the study is admittedly a high-level initial investigation of the overall problem, and much work remains. The subsystem failure types evaluated consisted of abrupt failures resulting in a complete loss of subsystem functionality. A practical failure mitigation approach would also require capabilities to mitigate more nuanced failure modes such as failures evolving more gradually or resulting in a partial loss of subsystem functionality. This might require blended control mode functionality and more sophisticated failure detection logic. Also, the study did not consider turbomachinery performance deterioration effects; it only considered turbomachinery of nominal (undeteriorated) health conditions. Further evaluation of the control design is needed to ensure that operability is maintained under all deterioration levels from nominal through end-of-life conditions. This study did consider an architectural change to the baseline STARC-ABL to facilitate failure mitigation that resulted in the power system being partitioned into two parallel strings. However, a more thorough systems engineering approach could likely identify additional architectural changes to provide added robustness and failure mitigation functionality.

## 8. CONCLUSIONS

A reversionary control strategy for maintaining operability of an electrified aircraft propulsion (EAP) concept in the presence of subsystem failures was presented. The approach was applied to a distributed partially turboelectric propulsion architecture consisting of two turbofan engines that produce thrust and supply mechanical offtake power for the generation of electricity supplied to a motor-driven tailfan propulsor. This effort demonstrated the operability concerns posed by subsystem failures in an EAP architecture that exhibits tight integration and coupling between subsystems. If unmitigated, such failures can cause engine compressor stalls, engine shutdowns, and cascading failures sometimes with catastrophic consequences. Presented failure detection logic and reversionary control modes included in the propulsion control system were shown to successfully mitigate the effects of such failures, allowing the system to continue to operate and produce thrust. A real-time hardware-in-the-loop test of the integrated control design demonstrated robust transient system operation in the presence of realistic electrical system variations.

## ACKNOWLEDGMENTS

This work was conducted under the NASA Advanced Air Vehicles Program, Advanced Air Transport Technology Project, Aircraft Electrification Subproject.

## REFERENCES


[1] Jansen, R.H., Bowman, C., Jankovsky, A., Dyson, R., Felder, J., (2017), "Overview of NASA Electrified Aircraft Propulsion Research for Large Subsonic Transports," AIAA-2017-4701, AIAA Propulsion and Energy Forum, Atlanta, GA, July 10-12.

[2] National Academies of Sciences, Engineering, and Medicine. 2016. Commercial Aircraft Propulsion and Energy Systems Research: Reducing Global Carbon Emissions. Washington, DC: The National Academies Press. https://doi.org/10.17226/23490.

[3] SAE International Aerospace Recommended Practice, (2010), "Guidelines for Development of Civil Aircraft and Systems," SAE Standard ARP4754A, December 2010.

[4] SAE International Aerospace Recommended Practice, (1996), "Guidelines and Methods for Conducting the Safety Assessment Process on Civil Airborne Systems and Equipment," SAE Standard ARP4761, December 1996.

[5] Courtin, C., Hansman, R.J., (2018), "Safety Considerations in Emerging Electric Aircraft Architectures," AIAA-2018-4149, Aviation Technology, Integration, and Operations Conference, Atlanta, GA, Jun. 25-29.

[6] Simon, D. L., and Connolly, J. W., (2020), "Electrified Aircraft Propulsion Systems: Gas Turbine Control Considerations for the Mitigation of Potential Failure Modes and Hazards," ASME-GT2020-16335, ASME Turbo Expo Conference, Virtual, Online, September 21-25.

[7] Zhang, D., Xu, Y., Zhang, Z., Dong, D., Cao, Y., Mcginnis, P., Keck, B. (2023), "A Solid-State Circuit Breaker for Hybrid Electric Propulsion," AIAA 2023-4155, AIAA Aviation Forum, San Diego, CA, Jun. 12-16.

[8] Flynn, M. C., Jones, C., Rakhra, P., Norman, P., and Galloway, S. (2017), "Impact of Key Design Constraints on Fault Management Strategies for Distributed Electrical Propulsion Aircraft," AIAA-2017-5034, 53rd AIAA/SAE/ASEE Joint Propulsion Conference, Atlanta, GA, Jul. 10-12.

[9] Kuhlberg, J. F., Newirth, D. M., Kniat, J., and Zimmerman, W. H. (1984), "Integration of the PW2037 Engine Electronic Control System in the Boeing 757 Airplane," SAE Technical Paper No. 841554, Aerospace Congress & Exposition, Long Beach, CA, Oct. 15-18.

[10] Bosco, C. J., "Certification Issues For Electrical and/or Electronic Engine Controls," SAE Paper 871844, Aerospace Technology. Conference and Exposition, Long Beach, CA, Oct. 5-8, 1987.

[11] Evans, J.F.O., "Fault Trees and System Reliability Analysis with Reference to the Control of Aircraft Engines," AGARD-LS-113, Microcomputer Applications in Power and Propulsion Systems, March 1981.

[12] Kratz, J. L., and Simon, D.L., (2024), "Failure Behavior and Control-Based Mitigation for a Parallel Hybrid Propulsion System," AIAA-2014-0522, AIAA SciTech Forum, Orlando, FL, Jan. 8-12.

[13] Kratz, J. L., and Simon, D.L., (2022), "Failure Modes and Mitigation Strategies for a Turboelectric Aircraft Concept with Turbine Electrified Energy Management," AIAA-2022-1191, AIAA SciTech Forum, San Diego, CA, Jan. 3-7.

[14] Welstead, J.R., Felder, J.L., (2016), "Conceptual Design of a Single-Aisle Turboelectric Commercial Transport with Fuselage Boundary Layer Ingestion," AIAA 2016-1027, AIAA SciTech Forum, 54th AIAA Aerospace Sciences Meeting, San Diego, CA, January 4-8.

[15] Felder, J. L., Schnulo, S. L., Tong, M. T., Berton, J. J., Thacker, R. P., Haller, W. J. (2022), "An Updated Assessment of Turboelectric Boundary Layer Ingestion Propulsion Applied to a Single-Aisle Commercial Transport," AIAA SciTech Forum and Exposition, San Diego, CA, January 3-7.

[16] Kratz, J. L., Culley, D. E., and Thomas, G. L., (2019), "A Control Strategy for Turbine Electrified Energy Management," AIAA–2019–4499 AIAA/IEEE Electric Aircraft Technologies Symposium (EATS), Indianapolis, Indiana, August 22–24.

[17] Litt, J.S., Sachs-Wetstone, J.J., Simon, D.L., Sowers, T.S., Owen, A.K., Bell, M.E., Guthrie, B.E., Lehan, J. and Castro, A., (2023), "Flight Simulator Demonstration and Certification Implications of Powertrain Failure Mitigation in a Partial Turboelectric Aircraft," AIAA 2023-4156, AIAA/IEEE Electrified Aircraft Technology Symposium (EATS), San Diego, CA, Jun. 12-16.

[18] Lytle, J., Follen, G., Naiman, C., Evans, A., Veres, J., Owen, K., Lopez, I., (2000), "Numerical Propulsion System Simulation (NPSS) 1999 Industry Review," NASA/TM-2000-209795, August.

[19] Simon, D.L., Bianco, S.J., Horning, M.A., (2023), "Integrated Control Design for a Partially Turboelectric Aircraft Propulsion System," ASME-GT2023-100921, ASME Turbo Expo Conference, Boston, MA, June 26-30.

[20] Chapman, J.W., Lavelle, T.M., May, R.D., Litt, J.S., Guo, T-H., (2014), "Toolbox for the Modeling and Analysis of Thermodynamic Systems (T-MATS) User's Guide," NASA/TM-2014-216638, January.

[21] Chapman, J.W., Litt, J.S., (2018), "An Approach for Utilizing Power Flow Modeling for Simulations of Hybrid Electric Propulsion Systems," AIAA-2018-5018, AIAA Propulsion and Energy Forum, Cincinnati, OH, July 9-11.

[22] Jaw, L., and Mattingly, J., (2009), "Aircraft Engine Controls," New York, NY, USA: American Institute of Aeronautics and Astronautics.

[23] May, R.D., Garg, S., (2012), "Reducing Conservatism in Aircraft Engine Response Using Conditionally Active Min-Max Limit Regulators," ASME GT2012-70017, ASME Turbo Expo, Copenhagen, Denmark, June 11-15.

[24] Scoles, R. J., 1986, "FADEC – Every Jet Engine Should Have One," SAE Paper 861802.

[25] Buescher, H.E., Culley, D.E., Bianco, S.J., Connolly, J.W., Dimston, A.E., Saus, J.R., Theman, C.J., Horning, M.A., and Purpera, N.C., (2023), "Hybrid-Electric Aero-Propulsion Controls Testbed: Overview and Capability," AIAA 2023-0671, AIAA SciTech Forum, January 23-27.

[26] Simon, D.L., Bianco, S. J., Horning, M.A., Saus, J.R., Amthor, A.E., Sachs-Wetstone, J.J., (2023), "Real-time Hardware-in-the-Loop Evaluation of a Partially Turboelectric Propulsion Control Design," AIAA 2023-4235, AIAA/IEEE Electric Aircraft Technologies Symposium (EATS), San Diego, California, June 12-16.

[27] Bianco, S.J., Simon, D.L., Hill, E.D, (2024), "Adaptive Control and Scaling Approach for the Emulation of Dynamic Subscale Torque Loads," AIAA-2024-2356, AIAA SciTech Forum, Orlando, FL, Jan. 8-12.